BBA Advances 4 (2023) 100101

Contents lists available at ScienceDirect

BBA Advances

journal homepage: www.sciencedirect.com/journal/bba-advances

Advances in chaperone-assisted RNA crystallography using synthetic antibodies

Hasan Al Banna, Naba Krishna Das, Manju Ojha, Deepak Koirala *

Department of Chemistry and Biochemistry, University of Maryland Baltimore County, Baltimore, MD 21250, USA

ARTICLE INFO

Keywords:
RNA structures
Synthetic anti-RNA Fab
X-ray crystallography
Crystallization chaperones
Fab-RNA complex
Fab-assisted RNA crystallography

ABSTRACT

RNA molecules play essential roles in many biological functions, from gene expression regulation, cellular growth, and metabolism to catalysis. They frequently fold into three-dimensional structures to perform their functions. Therefore, determining RNA structure represents a key step for understanding the structure-function relationships and developing RNA-targeted therapeutics. X-ray crystallography remains a method of choice for determining high-resolution RNA structures, but it has been challenging due to difficulties associated with RNA crystallization and phasing. Several natural and synthetic RNA binding proteins have been used to facilitate RNA crystallography. Having unique properties to help crystal packing and phasing, synthetic antibody fragments, specifically the Fabs, have emerged as promising RNA crystallization chaperones, and so far, over a dozen of RNA structures have been solved using this strategy. Nevertheless, multiple steps in this approach need to be improved, including the recombinant expression of these anti-RNA Fabs, to warrant the full potential of these synthetic Fabs as RNA crystallization chaperones. This review highlights the nuts and bolts and recent advances in the chaperone-assisted RNA crystallography approach, specifically emphasizing the Fab antibody fragments as RNA crystallization chaperones.

1. Introduction

RNAs are perhaps the most versatile biomacromolecules that play vital roles in myriad functions ranging from gene expression regulation, cell growth, and metabolism to catalysis [1–4]. These molecules often fold into complicated three-dimensional structures to perform their functions [5–8]. With recent advancements in high-throughput RNA identification and sequencing technologies, the discovery of new RNAs and their functions has increased enormously in recent years [9–12]. However, three-dimensional structure determination and characterization of RNA remain in their infancy compared to that of proteins. A detailed understanding of RNA structures not only helps to reveal mechanisms of biological processes but also facilitates the development of approaches targeting RNA to combat genetic and infectious diseases. Therefore, developing new techniques and strategies for RNA structural biology research has been a demanding challenge for transforming the overall RNA-centered research to synergize with the effective development of RNA-targeted treatments and cures.

In terms of the tendency to fold in similarly stable conformational states because of their intrinsic properties, biological RNA molecules can exist in more dynamic forms than proteins and DNAs [13–16], making RNA structural biology studies a difficult challenge. The first crystal structure of a synthetic RNA was reported in 1976 [17], and the complete turn of the A-form RNA helix (PDB ID: 1RNA) was determined in 1989 [18]. Nevertheless, the first crystal structure of a functional RNA, the yeast phenylalanine tRNA, was derived by multiple groups several years before the determination of the high-resolution crystal structure of the A-form RNA helix [19]. Over the past four decades since the 1980s, the field of RNA structural biology has continued to grow, uncovering valuable information about structures, folding dynamics, and mechanisms of RNA-based functions. However, the pace of RNA structure determination has been slower and left far behind compared to that of proteins. It is interesting that the crystal structures of the first protein and RNA were determined at about the same time, but the total number of RNA structures, compared to proteins, deposited in the protein databank (PDB) to date remains negligible. For example, according to PDB statistics, the total number of RNA-only structures released to date (May 2023) starting from the year 1978 is 1726, compared to 177,606 for protein structures starting from the year 1976. These RNA-only structures account for only about 1% of the total biomacromolecular

* Corresponding author.
E-mail address: dkoirala@umbc.edu (D. Koirala).

https://doi.org/10.1016/j.bbadva.2023.100101
Received 17 May 2023; Received in revised form 13 July 2023; Accepted 17 August 2023
Available online 19 August 2023

structures deposited in the PDB database (Fig. 1a). Even considering the protein complexes of nucleic acids (both RNA and DNA), these structures account only for about 5% of the total structures deposited into the PDB database. Consistently, the number of RNA-only structures released per year in the PDB database for the last 10 years (2013–2022) is 74 ± 14 (mean ± SD) compared to 9720 ± 1367 (mean ± SD) for proteins (Fig. 1b), reflecting the difficulties with RNA structure determination despite great recent advancements in the major structural biology methods such as X-ray crystallography, nuclear magnetic resonance (NMR) and cryogenic electron microscopy (cryoEM).

Although NMR and, more recently, cryoEM methods have been used for structural studies of biomolecules, X-ray crystallography so far has remained the most widely used and advanced method for determining the 3-dimensional structures of RNAs and other biomacromolecules (Fig. 1b, c). NMR has the advantage of being able to provide information about dynamics, but the complexity of the structure determination increases with the size of the RNA target, and thus, it is challenging to use this method to determine the structures of intact RNAs of biologically relevant size. Moreover, although it provides high-resolution structural information, NMR requires a high concentration of isotopically labeled samples, which is expensive and may result in undesirable intermolecular interactions. Consistent with these difficulties, there are only a few RNA structures larger than 100-nt RNAs that have been determined by NMR [20], usually in combination with other techniques such as small-angle X-ray scattering (SAXS) [21,22]. CryoEM has recently demonstrated tremendous progress in determining the three-dimensional structures of proteins and large protein-RNA complexes, such as ribosomes and spliceosomes [23–25]. Nevertheless, the cryoEM resolution revolution has not yet reached the level of NMR and X-ray crystallography, and especially, this method remains underdeveloped for standalone RNAs because of the unusual behavior of RNA molecules (electrostatics, thermodynamic stability, and folding) when applied to the cryoEM grids. Compared to NMR and cryoEM, X-ray crystallography offers several advantages. With several technically advanced synchrotron facilities available all around the world, it has been the method of choice for determining the high-resolution structures of various biomacromolecules, including RNAs with a broad spectrum of molecular size [26]. Nevertheless, high-resolution structure determination of RNAs by X-ray crystallography remains challenging due to inherent difficulties in crystallizing RNA molecules [27]. Compared to proteins with a chemically diverse surface (twenty amino acids) that assist lattice interactions and crystal packing, RNA has a limited surface diversity (only four nucleotides) with mutually repulsive, negatively charged phosphate groups along the backbone, which prevent efficient crystal packing [28,29]. Moreover, RNAs tend to adopt multiple conformations and create a heterogeneous sample, which will be counterproductive for the crystallization [30,31]. Additionally, obtaining phase information from RNA crystals is tedious and time-consuming due to the lack of facile strategies like heavy-atom derivatization, a common phasing strategy used in protein crystallography [32–35].

Over the past several years, various approaches have been developed to facilitate both RNA crystallization and crystallographic phase determination [29,35–38]. Approaches such as construct screening and engineering that help form crystal contacts and can support the growth of diffraction-quality crystals have been employed in RNA crystallography. Some RNA tertiary motifs like tetraloops and tetraloop receptors have proven important for creating robust crystal contacts because of their stable fold and chemical disposition towards long-range interactions. For example, the crystallography of hepatitis delta virus (HDV) ribozyme was significantly improved for the constructs containing engineered GNRA tetraloop and tetraloop receptors [39,40]. Because the crystal structures of tRNAs have shown high topological conservation and ability to generate well-defined higher-order scaffolds [41], the fusion of RNA target with tRNA scaffold has been shown to enhance the rate of crystal formation significantly. The mutations to the anticodon loop, the acceptor stem, and the stacking surface of the D and T loops in the tRNA molecule can create suitable intermolecular interactions for RNA crystal growth without altering the tRNA scaffold structure [38]. Such knowledge of well-characterized tRNA interactions will certainly aid in designing RNA-tRNA fusion crystallization constructs, interpreting the electron density maps, refinement, and modeling. The robust stability and folding of a tRNA make the phasing by a molecular replacement simple, making tRNA a good crystallization chaperone. The structures of pro-head RNA domain II [42] and T-box riboswitch [43] have been successfully determined with the fusion of tRNA as a crystallization chaperone. However, these direct engineering approaches are RNA target specific and require extensive construct designs and

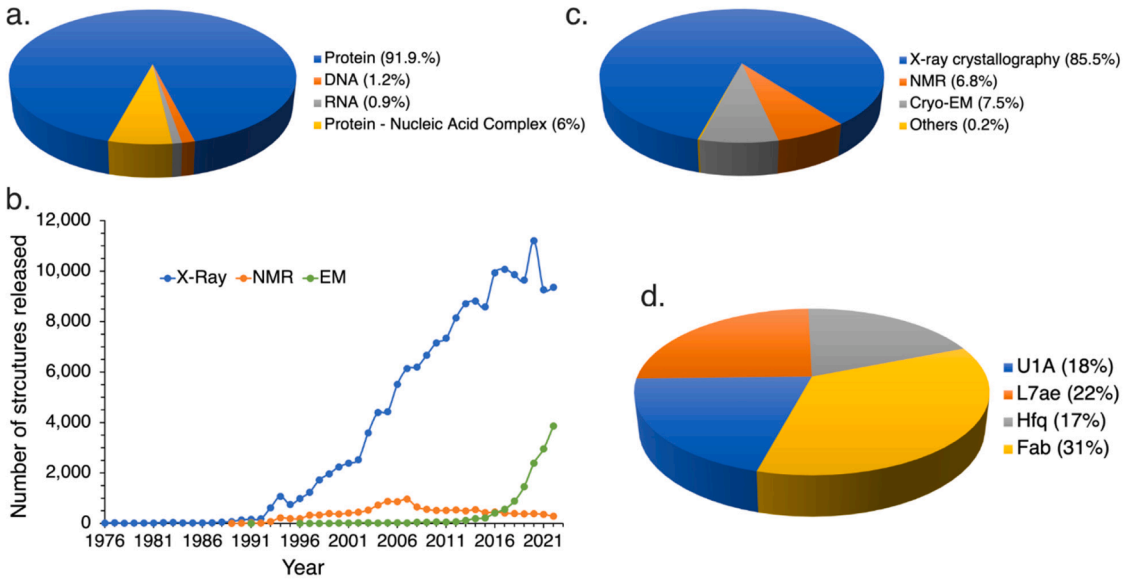

Fig. 1. Statistics of the biomacromolecular structures deposited in the PDB. (a) The total number of structures (percentages) released in the PDB as of May 2023 categorized by macromolecule types. (b) The number of macromolecular structures released per year in the PDB from 1976 to 2023, and (c) the proportional numbers as of May 2023 based on the major macromolecular structure determination methods. (d) The relative numbers of RNA-chaperone complex structures released in the PDB as of May 2023 determined by using various chaperones through chaperone-assisted RNA crystallography.

screening.

Other promising approaches use RNA-binding proteins as crystallization chaperones. The protein binding RNA motif is grafted into the target RNA, enabling the complex formation and, thus, allowing subsequent crystallography of the chaperone-RNA complex rather than the RNA alone. These chaperones can be mainly categorized into two broad classes, natural RNA binding proteins (RBPs), such as U1A RNA binding protein and a family of L7Ae proteins, and synthetic protein chaperones, such as Fab (fragment antigen-binding) fragments. The chaperone-assisted RNA crystallography has proven to be a successful approach for determining the crystal structures of RNA. So far, more than one hundred RNA crystal structures deposited in the PDB database have been determined by using some types of crystallization chaperones. Fig. 1d compares the percentages of crystal structures solved using different chaperones, and Table 1 lists some notable RNA structures solved by using such chaperone-assisted RNA crystallography. With extensive surface chemical diversity and pre-determined high-resolution crystal structures, the protein chaperones offer various advantages that help minimize RNA-RNA contacts in the crystal lattice, stabilize the flexible regions within the RNA, and provide initial phase determination via molecular replacement. In the following sections, we will briefly discuss various natural and synthetic protein chaperones used for RNA crystallization and a more detailed discussion on procedures, applications, and limitations of Fabs as RNA crystallization chaperones.

2. Natural RNA binding proteins as crystallization chaperones

As the crystallization chaperones, proteins introduce a chemically distinct surface that can facilitate crystal packing and yield diffracting crystals. Several naturally occurring RNA binding proteins have been identified that have the potential to serve as RNA crystallization chaperones. These proteins have portable RNA epitopes and can be engineered into the target RNA as affinity tags, allowing downstream crystallographic processing with the protein-RNA complexes. The choice of a protein chaperone module for a new RNA target depends on a wide variety of factors, such as the size of the target RNA, the nature of the epitope engineering site (*i.e.*, loop, bulges, k-turns, or single-stranded regions), and sometimes on the laboratory-specific resources. While a trial-and-error has been a classical approach, bigger chaperones relative to the target RNA to be crystallized have been more useful in our hands, perhaps due to a greater surface area of the protein available for the crystal contacts. Importantly, having a significant portion of the chaperone in the RNA-chaperone complex greatly facilitates the phasing through molecular replacement. We have discussed below some RNA binding proteins used in RNA crystallography, with some examples of RNA crystal structures determined using these chaperones (Fig. 2).

Table 1
Some examples of commonly used RNA crystallization chaperones with corresponding RNA structures solved using chaperone-assisted RNA crystallography. The listed molecular weight (MW) values represent that of the monomeric protein.

Chaperone	Type	MW (kDa)	Some examples of solved RNA structures
Fab	Synthetic RBP	~ 50	6XJZ [49], 2R8S [50], 6DB9 [51], 7SZU [52], 8D29 [53], 3IVK [54], 6B14 [55], 6MWN [56], 4KZD [57], 7MLX [58], 6U8D [59], 6 × 5M [60], 8DP3 [48]
U1A	Natural RBP	~ 11	4PR6 [61], 7D7V [47], 6CMN [62], 5DDO [63], 4W90 [64], 4YB1 [65,66], 5FJ4 [66], 4PKD [67]
L7Ae	Natural RBP	~ 13	1RLG [68], 7OZQ [69], 4C4W [70], 4BW0 [44], 5G4U [71], 5DCV [72], 1SDS [73], 6Q8U [74], 3PLA [75], 3HAX [76]
Hfq	Natural RBP	~ 9	1kQ2 [77], 3GIB [78], 3HSB [79], 3QSU [80], 3RER [81], 4NL3 [82], 4QVC [83], 4V2S [46], 5NEW [84], 5SZE [85]
tRNA	RNA scaffold	~ 25	4TZZ [86], 4MGN [87], 6PMO [45], 6UFG [88], 6UFM [89]

2.1. U1A RNA binding protein

The spliceosomal U1 RNA binding protein (U1A) is the first and, a commonly used chaperone for RNA crystallization. It recognizes an RNA hairpin loop sequence (AUUGCACUCC) through its RNA recognition motif (RRM) [90]. The RNA–protein binding interface is comprised of polar and non-polar interactions [91], which makes this protein stable in both low and high ionic strengths, enabling it to be used as a crystallization module in various conditions. U1A protein binds with cognate RNA with very high affinity (dissociation constant, $K_d \sim 20$ pM) [92,93]. It folds as a compact, globular domain, which is favorable for packing U1A molecules in the crystal lattice. The U1A was first used for crystallizing the hepatitis delta virus (HDV) ribozyme [39], and soon after, several other RNA structures were determined using this module as a crystallization chaperone [90,94,95]. Besides serving as a molecular replacement model, the U1A protein surface has also provided opportunities for using traditional approaches for phasing. For example, incorporating Selenomethionine residues in the U1A protein has provided initial phase information for U1A-RNA crystals for determining the crystal structures of tetracycline aptamer and TPP riboswitch RNAs [90,91]. Nevertheless, the size of the U1A (MW ~ 11 kDa) [55] compared to the RNA target to be crystallized pose a critical challenge for the crystallography of the U1A-RNA complexes.

2.2. Kink-turn RNA binding protein

The kink-turns (known as K-turns) are frequent motifs in RNA structures, which are known to bind the L7Ae family of proteins naturally. The K-turn motifs bend the RNA double helix by about the right angle, and therefore, these proteins essentially stabilize the tightly kinked RNA structure. These proteins bind the K-turn motifs with very high affinity ($K_d \sim 10$ pM) [96], the RNA epitope motif is structurally conserved and can be easily added to the peripheral helical components within the target RNA, and the L7Ae homologs are abundant with various molecular characteristics, making these K-turn RNA and protein modules a general chaperone for RNA crystallography [97]. Some prominent examples of RNA crystal structures solved by using this chaperone system include the T-box riboswitch in complex with YbxF [43] (L7Ae homolog) and Kt-23 RNA in complex with an L7Ae protein [70]. Remarkably, this chaperone was modified to include Selenomethionines for acquiring the phase information and determining the crystal structure of an mRNA-tRNA complex [43]. However, the relatively smaller size of the L7Ae proteins (MW ~ 15 kDa) [55] and the requirement of tagging the RNA target within the RNA helix brings several complications, such as the stability and conformation of the RNA structures, reflecting significant challenges in using this K-turn-L7Ae chaperone system.

2.3. RNA binding protein HFQ

The Hfq protein is a replication host factor of an RNA virus, the bacteriophage Qbeta, that has an important role in the post-transcriptional gene regulation by small non-coding RNAs (sRNAs) [98]. The Hfq protein has a hexameric fold in which the proximal face recognizes the poly-U sequences of sRNAs, and the distal face binds with the mRNA poly-A tails [77,78,99], bringing these two RNA regions into proximity. Although this protein has shown promising results as an RNA crystallization chaperone by establishing the intermolecular interactions that assisted a stable crystal lattice formation [85], its full potential as an RNA crystallization chaperone is yet to be explored. Nevertheless, the ability of the Hfq protein to self-assemble into hexameric forms and the availability of its numerous homolog proteins with three-dimensional structures offer some advantages of using this

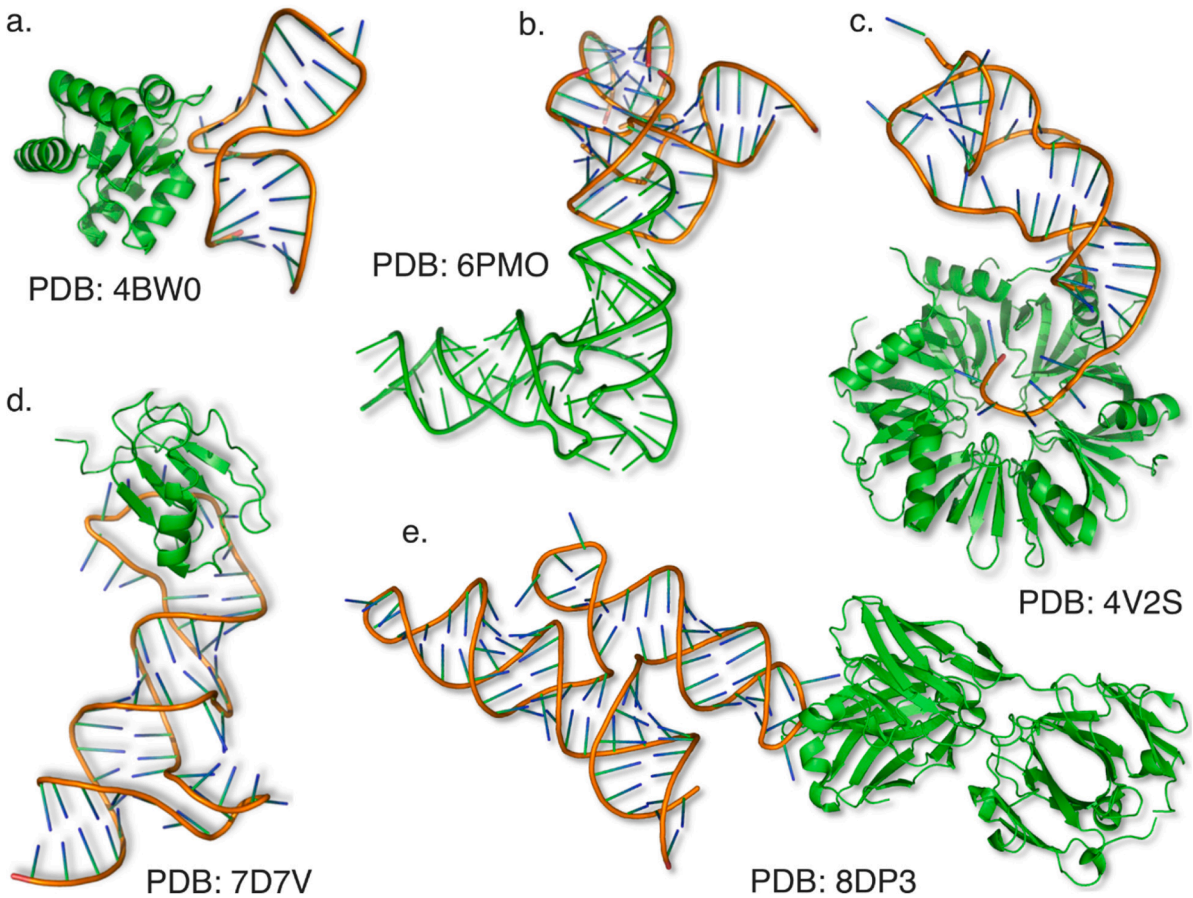

Fig. 2. Representative structures of RNA-chaperone complexes solved by chaperone-assisted RNA crystallography. (a) The L7Ae with a kink-turn RNA structure (PDB ID: 4BW0) [44], (b) the tRNA scaffold as a chaperone for T-Box riboswitch structure determination (PDB ID: 6PMO) [45], the Hfq chaperone in complex with the sRNA RydC (PDB ID:4V2S) [46], the U1A RBP with NAD^+ riboswitch (PDB ID: 7D7V) [47], and the Fab BL3-6 chaperone in complex with CVB3 RNA replication domain (PDB ID: 8DP3) [48].

chaperone for RNA crystallization and structure determination. However, the flexible epitope (*i.e.*, single-stranded poly-U and poly-A sequences) and relatively weaker affinity to the relatively larger RNA epitope (Kd ~1.2 nM) [85] compared to the U1A and L7Ae proteins are some potential problems in using Hfq as an RNA crystallization chaperone.

3. Synthetic antibody fragments as RNA crystallization chaperones

The most notable recent progress in the chaperone-assisted RNA crystallography field is the development of anti-RNA Fabs (antigen-binding fragments). Fab chaperones offer multiple advantages over traditional ones, such as U1A and L7Ae RNA binding protein, including larger size, greater surface area for crystal lattice interactions, and higher beta-rich structure for the self-association using accessible beta-sheet edges. For example, U1A and L7Ae have an approximate molecular weight of ~11 kDa and ~13 kDa, a β-sheet component of 21% and 17%, and a total solvent accessible surface area (SASA) of 5223 $Å^2$ and 6314 $Å^2$. On the other hand, the Fab scaffold has a molecular weight of about 50 kDa (about four times higher than U1A and L7Ae), the β-sheet component ~48%, and SASA ~38,712 $Å^2$ (about six times higher SASA than U1A and L7Ae) [55]. Because of the large and well-defined globular fold, the Fab scaffolds have been highly effective search models for molecular replacement. Typically, the anti-RNA Fabs against the RNA targets are selected *in vitro* from synthetic Fab libraries using a phage display selection [50]. However, once the Fab binders for an RNA are identified, related RNA epitopes can be turned into portable motifs to create a portable chaperone-tag system [103]. The RNA epitope then can be grafted into other RNA targets, which allows complex formation with the chaperone, allowing crystallization of the chaperone-RNA complex. Some of the most recent RNA crystal structures determined using this Fab-assisted approach are the Spinach RNA aptamer [57], hepatitis A virus (HAV) IRES domain V [56], a self-alkylating ribozyme [49], and coxsackievirus B3 replication-linked cloverleaf domain [48]. Fig. 3 shows the structures of RNA solved in complex with their respective Fab binders selected directly through the phage display selection [50,54,56,59,100]. Some Fabs, such as BL3–6 and HAVx, have been transformed into portable modules to crystallize different RNA targets [48,49,51,52,55,58,60,101,102]. In all Fab-RNA complex structures, including the binding interface, Fab mediated most of the crystal contacts (*i.e.*, nominal RNA-RNA contacts), underscoring the robustness of Fab chaperones for facilitating RNA crystallography (Fig. 3f). In the following sections, we have discussed general experimental considerations and guidelines for using Fab chaperones for RNA crystallization and structure determination.

4. General workflow and experimental approaches in Fab-assisted RNA crystallography

As natural antibodies against RNA targets are rare, developing anti-RNA antibodies through the host immunization approach is extremely challenging. Recent technologies such as phage display selection have provided great opportunities for selecting anti-RNA antibody fragments, such as Fabs from the synthetic Fab displaying phage libraries *in vitro* [50,103]. Thus, the bottleneck of the Fab-assisted RNA crystallography

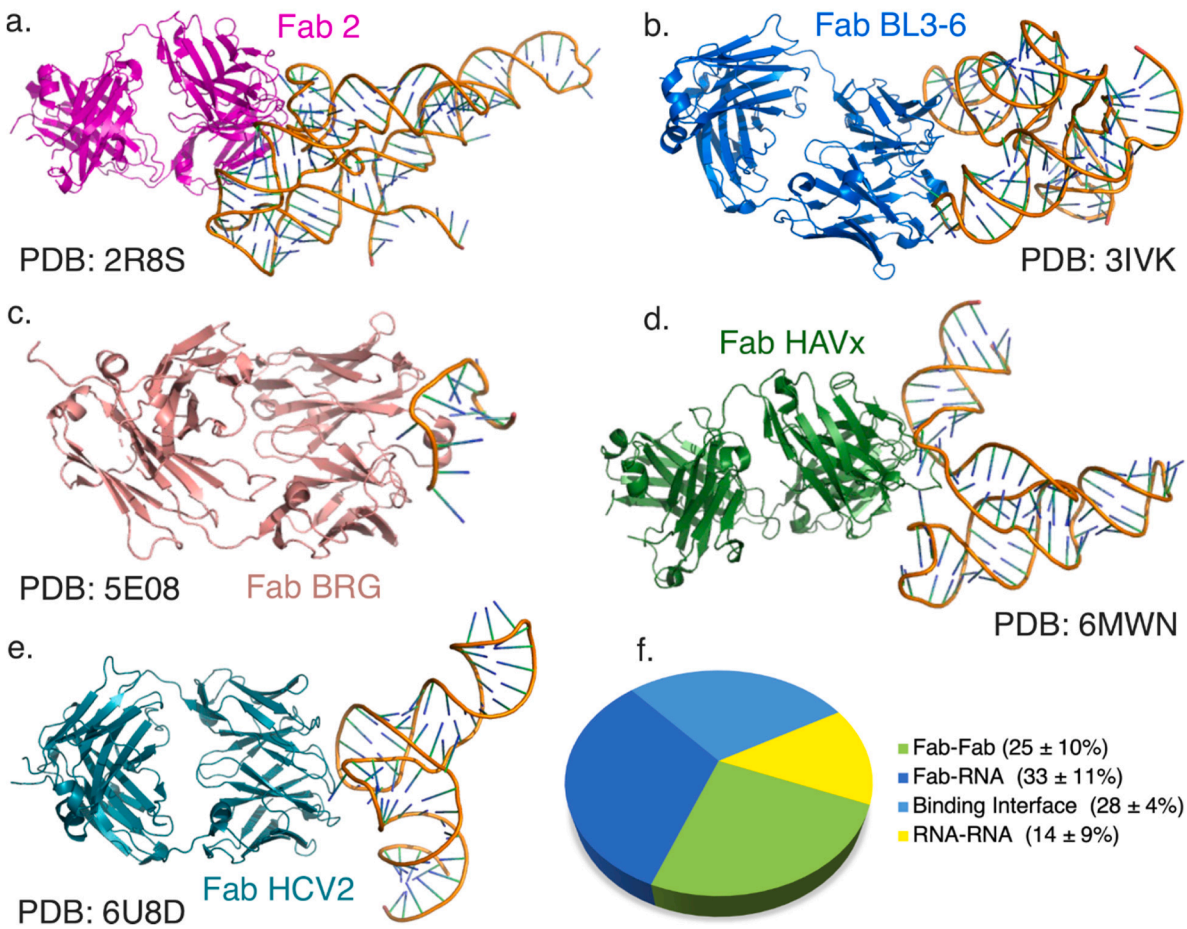

Fig. 3. Some examples of RNA structures determined by Fab-assisted RNA crystallography. (a) The P4-P6 ribozyme domain in complex with Fab 2 (PDB ID: 2R8S) [50], (b) the class I ligase ribozyme in complex with Fab BL3-6 (PDB ID: 3IVK) [54], a single-stranded RNA in complex with Fab BRG (PDB ID:5EO8) [100], the domain V RNA from HAV IRES in complex with Fab HAVx (PDB ID: 6MWN) [56], and the JIIIabc RNA from HCV IRES in complex with Fab HCV2 (PDB ID: 6U8D) [59]. The specific Fab was obtained against the RNA target through phage display selection. Portable epitopes have been developed for Fab BL3-6 and HAVx and used subsequently for determining crystal structures of various RNA structures through the epitope tagging approach [48,49,51,52,55,58,60,101,102]. (f) The percentages of crystal contacts calculated from over a dozen Fab-RNA complexes show that Fab mediates most of the contacts in the Fab-RNA complex crystals.

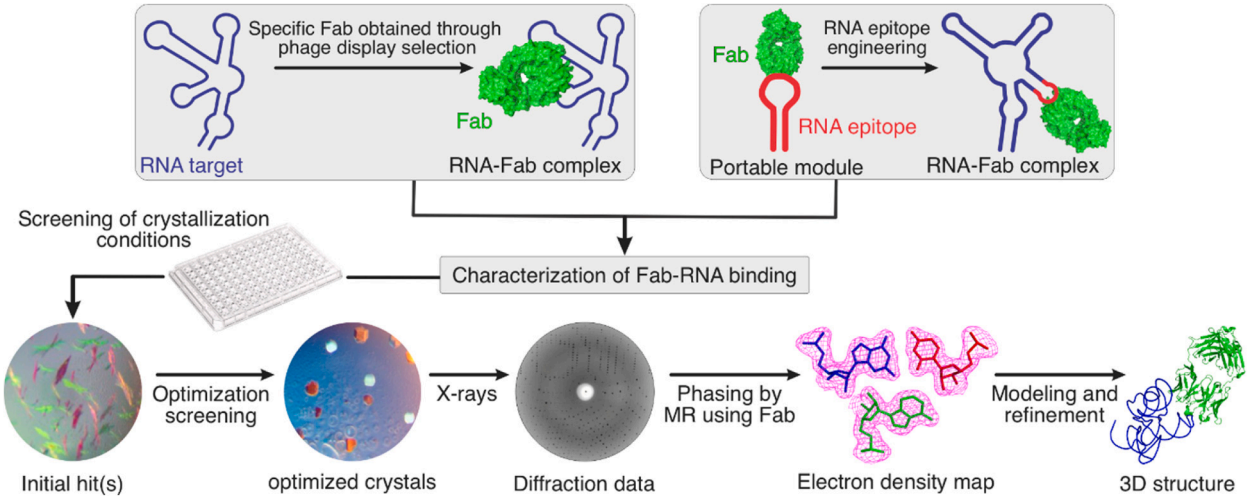

Fig. 4. General approaches and experimental workflow of Fab-assisted RNA crystallography. The RNA-Fab complex for the target RNA can be prepared through two approaches: using Fab(s) obtained through phage display selection against the target and engineering portable epitopes to tag the target RNA with a Fab-binding sequence. After the characterization of the Fab-RNA binding, the Fab-RNA complex is advanced to the standard crystallography pipeline to solve the crystal structure of the Fab-RNA complex, where Fab is used as a search model for initial phasing via molecular replacement.

relies upon the successful selection of anti-RNA Fab(s) against the crystallization RNA target(s). Once the Fab binders are selected, and the Fab-RNA interactions characterized, the resulting Fab-RNA complexes are advanced to the crystallographic pipeline. However, the phage display selection for every crystallization RNA target is technically challenging, laborious, and expensive. More recently, to bypass phage display selection for each RNA crystallization target, an *in vitro* selection approach was used to develop multiple mobile Fab-tag modules [55] that can be grafted into the new crystallization RNA target as tags. Engineering of such a Fab binding tag enables complex formation with the Fab, allowing the subsequent crystallization of the Fab-RNA complex. This approach has successfully determined the crystal structures of diverse RNA targets such as Spinach RNA aptamer [101] and a self-alkylating ribozyme [49]. A suite of these modules with Fabs that bind their cognate RNAs with different orientations has been developed that allows screening multiple crystallization constructs for a single RNA target, offering multiple shots on goal. As details of phage display selection against RNA targets have been reviewed elsewhere [50,103], this review focuses on the procedures and key steps that need to be considered when using Fabs as RNA crystallization chaperones, regardless of the approach (direct selection of the Fab or engineering of Fab binding sequence), and some potential approaches for troubleshooting. Fig. 4 shows a schematic of key steps in the Fab-assisted RNA crystallography workflow.

4.1. RNA construct design for crystallization

The native sequence of the target RNA often needs to be modified for crystallization to reduce flexibility and improve homogeneous folding. However, such modifications must not impair the function of that RNA. The crystallization RNA construct design includes the replacement of poorly conserved flexible nucleotide(s) with stabilizing mutations or stable helices, unstructured loops with stable GNRA-type tetraloops, and the use of sequences from different species [26]. The secondary structure prediction algorithms, such as mFold [104] that predict the thermodynamic stability of potential secondary structures are very useful in assisting the construct design. Typically, the functionally dispensable loops are replaced with Fab-binding tag sequence(s) to create the Fab-binding site within the target RNA.

4.2. RNA synthesis and purification

The crystallization RNA constructs are typically synthesized by *in vitro* run-off transcription using linearized plasmid or PCR-generated DNA templates. The T7 RNA polymerase has been an enzyme of choice for transcription, which can be easily prepared recombinantly or purchased from commercial vendors. However, there are some limitations to using T7 polymerase for *in vitro* transcription. First, it requires guanine to be the first nucleotide in the transcript, and second, it tends to add extra nucleotides at the 3′end in the run-off transcriptions [105], generating the heterogeneous 3′ends in the transcript. The use of 2′O-methoxy modified reverse primers during DNA template preparation through PCR is helpful to minimize transcription heterogeneity at the 3′end [106]. Other approaches to creating homogeneous 5′ or 3′ ends include incorporation of the self-cleaving ribozyme sequences that flank the RNA sequence of interest, where the ribozyme cleaves the transcript at the desired position *in situ*, yielding the target RNA with homogenous ends [107–109].

In vitro transcribed RNA can be purified natively or denatured. The DNA template and enzymes from the transcription mixture can be removed using Phenol/Chloroform/Isopropanol (PCI) extraction at pH 4.5, and the recovered RNA can be buffer-exchanged or concentrated using appropriate molecular weight cut-off columns. For denaturing purification, it can be achieved simply via ethanol precipitation. The RNA is then purified by a large denaturing polyacrylamide gel electrophoresis (PAGE) or a native SEC (size-exclusion chromatography). The RNA band in the gel can be visualized by UV shadowing, excised, and extracted by a crush and soak method.

4.3. Fab expression and purification

Fab-assisted RNA crystallography approach requires a large quantity of high-quality, RNase-free, and soluble Fab proteins. As detailed protocols have been described elsewhere [56], we discuss here the main steps and limitations of the current Fab expression and purification strategies. The expression plasmid consists of two separate open reading frames corresponding to the light chain and heavy chain of the Fab. The anti-RNA Fab antibodies are expressed in the periplasm of 55244 *E. coli* cells. The induction of protein expression requires the phosphate-depleted media, and therefore, the growth media, which is typically a 2xYT, needs to be exchanged with the phosphate-depleted media to induce overexpression of the Fab. As these Fabs do not have purification tags, the affinity chromatography with consecutive use of protein-A, protein-G, and heparin columns has been successful. Nevertheless, Fab expression and purification steps are laborious, time-consuming, and expensive compared to conventional recombinant protein expression systems. The development of an expression system with robust inducible promotors that do not require growth media exchange will be helpful in saving time, labor, and reagents. The *E. coli* cells designed to facilitate cytoplasmic expression of proteins with disulfide bonds, such as Origami B cells, may help skip the periplasmic expression. Several cleavable tags can be used for easy and quick chromatographic purification to increase the overall yield. Yet, these expression systems need to be studied systematically.

4.4. RNA refolding and preparation of Fab-RNA complex

Unless purified natively, RNA constructs are required to be refolded in the desired buffer. The homogeneity of the refolded RNA samples can be confirmed by native PAGE and SEC. The refolded RNA conformation can be analyzed through binding tests with its native binding partners, such as fluorophores, metabolites, and proteins. The binding studies of RNA construct with Fab and the homogeneity of the Fab-RNA complexes can then be evaluated using conventional methods such as PAGE, SEC, and ITC (isothermal titration calorimetry). It is also critical to test whether the insertion of the Fab binding motif and subsequent binding of the Fab has disrupted the RNA's native structure and function, which can also be performed through binding tests with the target RNA's native binding partners, if any, such as metabolites or protein factors. Additionally, it is important to access information about the RNA secondary structures through available biochemical probing, bioinformatics, and consensus sequences. For the constructs that produce heterogeneous RNA (misfolding) and Fab-RNA complexes, troubleshooting includes the screening of refolding conditions by varying buffers, annealing protocol (snap cooling or slow cooling), identifying the flexible regions through biochemical analysis such as SHAPE [110] and in-line probing [91], and mutate those dynamic nucleotides or regions to minimize the flexibility. Once Fab-RNA binding is optimized, Fab-RNA complex with a final concentration of about 15–20 mg/ml (typically, 5–6 mg/ml of RNA in the complex). To ensure the homogeneity of the Fab-RNA complex, it can be further purified through SEC. Finally, the complex is filtered through a 0.2 μm filter to remove any aggregations or crystal seeds.

4.5. Crystallization of Fab-RNA complex

The well-characterized Fab-RNA (and Fab-RNP, if applicable) complexes are subjected to crystallographic screening. This is typically performed using a nanopipette robotic system with commercially available crystal screening kits. It is helpful to keep in mind that, unlike protein samples, RNA is a polyanionic molecule that has less sensitive acid-base titratable groups, and therefore, crystallization conditions and

crystal quality are very dependent on the cations present but less sensitive to pH change [26]. Therefore, the choice of screening conditions may increase the chance of RNA crystallization. Once initial crystal hits are observed, the condition(s) are further optimized for pH, salt, and precipitant concentration to grow and reproduce larger crystals using either the hanging or sitting drop vapor diffusion method. Other methods and approaches, such as seeding [111] and dehydration [86] of the crystals, might also be helpful for optimization and improving the diffraction quality. The fully grown crystals are then harvested with cryoprotectant and flash-frozen in liquid nitrogen. Although home X-ray sources have been used to screen and collect X-ray diffraction data sets, most laboratories use synchrotron facilities to screen and collect the X-ray diffraction data for biomacromolecular crystals, including the Fab-RNA complexes.

4.6. Structure solving and analysis

After collecting X-ray crystallographic diffraction patterns, the data analysis is performed using standard approaches. Most laboratories use standard software such as CCP4 [112], Phenix [113], and Coot [114] to analyze, build, and iteratively refine structural models. For solving the structure, one of the major advantages of using Fabs as crystallization chaperones is that previous Fab structures can provide initial phase information via molecular replacement. It is noteworthy that all Fab-RNA complex structures reported so far were solved by using Fab scaffolds as molecular replacement models. Although it remains to be investigated, Fabs could also offer opportunities to incorporate heavy residues such as Selenomethionine to facilitate phasing through conventional approaches.

5. Summary and future perspectives

RNAs are highly dynamic biomolecules with negatively charged surfaces that make their structure determination using X-ray crystallography extremely challenging. Both natural and synthetic RNA binding proteins have been proven helpful in facilitating RNA crystallization and structure determination. However, only a limited number of RNA-binding proteins have been explored for chaperone-assisted RNA crystallography. The development of a wide range of chaperone proteins, including the Fabs that bind RNA targets with different orientations, could increase the throughput and shots on goal for RNA crystallization and high-resolution structure determination. With the unique properties of Fabs to serve as crystallization chaperones, several RNA crystal structures, including ribozymes, riboswitches, aptamers, and viral RNA domains, have been solved recently using this strategy. Nevertheless, Fab expression and purification is laborious and technically challenging, and therefore, the development of a robust recombinant expression system for such anti-RNA Fabs is needed urgently to uncover the true potential of these synthetic antibodies as RNA crystallography chaperones. Although RNAs often function as RNP complexes, the application of the Fab approach for RNP crystallography is still unknown, and thus, integration of this powerful technology to crystallize and determine the various RNP structures will significantly benefit the RNA structural biology field.

Declaration of Competing Interest

The authors declare that they have no known competing financial interests or personal relationships that could have appeared to influence the work reported in this paper.

Data availability

Data will be made available on request.

Acknowledgements

This work was supported by University of Maryland Baltimore County (UMBC) start-up funds, and the NSF CAREER Award (MCB-2236996) to DK.

References

[1] A. Serganov, D.J. Patel, Ribozymes, riboswitches and beyond: regulation of gene expression without proteins, Nat. Rev. Genet. 8 (10) (2007) 776–790.
[2] T.A. Cooper, L. Wan, G. Dreyfuss, RNA and disease, Cell 136 (4) (2009) 777–793.
[3] J.S. Mattick, The genetic signatures of noncoding RNAs, PLos Genet. 5 (4) (2009), e1000459.
[4] T.R. Cech, J.A. Steitz, The noncoding RNA revolution-trashing old rules to forge new ones, Cell 157 (1) (2014) 77–94.
[5] A. Serganov, D.J. Patel, Metabolite recognition principles and molecular mechanisms underlying riboswitch function, Annu. Rev. Biophys. 41 (2012) 343–370.
[6] R.M. Voorhees, V. Ramakrishnan, Structural basis of the translational elongation cycle, Annu. Rev. Biochem. 82 (2013) 203–236.
[7] S.A. Mortimer, M.A. Kidwell, J.A. Doudna, Insights into RNA structure and function from genome-wide studies, Nat. Rev. Genet. 15 (7) (2014) 469–479.
[8] Q. Vicens, J.S. Kieft, Thoughts on how to think (and talk) about RNA structure, Proc. Natl Acad. Sci. 119 (17) (2022), e2112677119.
[9] J.G. Underwood, A.V. Uzilov, S. Katzman, C.S. Onodera, J.E. Mainzer, D. H. Mathews, T.M. Lowe, S.R. Salama, D. Haussler, FragSeq: transcriptome-wide RNA structure probing using high-throughput sequencing, Nat. Methods 7 (12) (2010) 995–1001.
[10] J.B. Lucks, S.A. Mortimer, C. Trapnell, S. Luo, S. Aviran, G.P. Schroth, L. Pachter, J.A. Doudna, A.P. Arkin, Multiplexed RNA structure characterization with selective 2′-hydroxyl acylation analyzed by primer extension sequencing (SHAPE-Seq), Proc. Natl Acad. Sci. 108 (27) (2011) 11063–11068.
[11] Y. Ding, Y. Tang, C.K. Kwok, Y. Zhang, P.C. Bevilacqua, S.M. Assmann, *In vivo* genome-wide profiling of RNA secondary structure reveals novel regulatory features, Nature 505 (7485) (2014) 696–700.
[12] J.M. Watts, K.K. Dang, R.J. Gorelick, C.W. Leonard, J.W. Bess Jr., R. Swanstrom, C.L. Burch, K.M. Weeks, Architecture and secondary structure of an entire HIV-1 RNA genome, Nature 460 (7256) (2009) 711–716.
[13] H.M. Al-Hashimi, N.G. Walter, RNA dynamics: it is about time, Curr. Opin. Struct. Biol. 18 (3) (2008) 321–329.
[14] A.M. Mustoe, C.L. Brooks, H.M. Al-Hashimi, Hierarchy of RNA functional dynamics, Annu. Rev. Biochem. 83 (2014) 441–466.
[15] S.L. Bonilla, J.S. Kieft, The promise of cryo-EM to explore RNA structural dynamics, J. Mol. Biol. 434 (18) (2022), 167802.
[16] M.L. Ken, R. Roy, A. Geng, L.R. Ganser, A. Manghrani, B.R. Cullen, U. Schulze-Gahmen, D. Herschlag, H.M. Al-Hashimi, RNA conformational propensities determine cellular activity, Nature 617 (7962) (2023) 835–841.
[17] N.C. Seeman, J.M. Rosenberg, F.L. Suddath, J.J. Kim, A. Rich, RNA double-helical fragments at atomic resolution. I. The crystal and molecular structure of sodium adenylyl-3′,5′-uridine hexahydrate, J. Mol. Biol. 104 (1) (1976) 109–144.
[18] A.C. Dock-Bregeon, B. Chevrier, A. Podjarny, J. Johnson, J.S. de Bear, G. R. Gough, P.T. Gilham, D. Moras, Crystallographic structure of an RNA helix: [U (UA)6A]2, J. Mol. Biol. 209 (3) (1989) 459–474.
[19] M. Jaskolski, Z. Dauter, A. Wlodawer, A brief history of macromolecular crystallography, illustrated by a family tree and its Nobel fruits, FEBS J. 281 (18) (2014) 3985–4009.
[20] D.C. Lawrence, C.C. Stover, J. Noznitsky, Z. Wu, M.F. Summers, Structure of the intact stem and bulge of HIV-1 Psi-RNA stem-loop SL1, J. Mol. Biol. 326 (2) (2003) 529–542.
[21] Y. Miyazaki, R.N. Irobalieva, B.S. Tolbert, A. Smalls-Mantey, K. Iyalla, K. Loeliger, V. D'Souza, H. Khant, M.F. Schmid, E.L. Garcia, A. Telesnitsky, W. Chiu, M. F. Summers, Structure of a conserved retroviral RNA packaging element by NMR spectroscopy and cryo-electron tomography, J. Mol. Biol. 404 (5) (2010) 751–772.
[22] G. Cornilescu, A.L. Didychuk, M.L. Rodgers, L.A. Michael, J.E. Burke, E. J. Montemayor, A.A. Hoskins, S.E. Butcher, Structural analysis of multi-helical RNAs by NMR-SAXS/WAXS: application to the U4/U6 di-snRNA, J. Mol. Biol. 428 (5 Pt A) (2016) 777–789.
[23] K. Zhang, S.C. Keane, Z. Su, R.N. Irobalieva, M. Chen, V. Van, C.A. Sciandra, J. Marchant, X. Heng, M.F. Schmid, D.A. Case, S.J. Ludtke, M.F. Summers, W. Chiu, Structure of the 30 kDa HIV-1 RNA dimerization signal by a hybrid Cryo-EM, NMR, and molecular dynamics approach, Structure 26 (3) (2018) 490–498, e3.
[24] K. Zhang, S. Li, K. Kappel, G. Pintilie, Z. Su, T.C. Mou, M.F. Schmid, R. Das, W. Chiu, Cryo-EM structure of a 40 kDa SAM-IV riboswitch RNA at 3.7 Å resolution, Nat. Commun. 10 (1) (2019) 5511.
[25] Z. Su, K. Zhang, K. Kappel, S. Li, M.Z. Palo, G.D. Pintilie, R. Rangan, B. Luo, Y. Wei, R. Das, W. Chiu, Cryo-EM structures of full-length Tetrahymena ribozyme at 3.1 Å resolution, Nature 596 (7873) (2021) 603–607.
[26] B.L. Golden, C.E. Kundrot, RNA crystallization, J. Struct. Biol. 142 (1) (2003) 98–107.
[27] A. Ke, J.A. Doudna, Crystallization of RNA and RNA-protein complexes, Methods 34 (3) (2004) 408–414.

[28] A.L. Edwards, A.D. Garst, R.T. Batey, Determining structures of RNA aptamers and riboswitches by X-ray crystallography, Methods Mol. Biol. 535 (2009) 135–163.
[29] J. Zhang, A.R. Ferre-D'Amare, New molecular engineering approaches for crystallographic studies of large RNAs, Curr. Opin. Struct. Biol. 26 (2014) 9–15.
[30] J.K. Flores, J.L. Walshe, S.F. Ataide, RNA and RNA–protein complex crystallography and its challenges, Aust. J. Chem. 67 (12) (2014) 1741–1750.
[31] A. Gomez, N. Toor, Selecting new RNA crystal contacts, Structure 26 (9) (2018) 1166–1167.
[32] V. Olieric, U. Rieder, K. Lang, A. Serganov, C. Schulze-Briese, R. Micura, P. Dumas, E. Ennifar, A fast selenium derivatization strategy for crystallization and phasing of RNA structures, RNA 15 (4) (2009) 707–715.
[33] J. Lu, P.D. Sun, A rapid and rational approach to generating isomorphous heavy-atom phasing derivatives, FEBS J. 281 (18) (2014) 4021–4028.
[34] A.C. Pike, E.F. Garman, T. Krojer, F. von Delft, E.P. Carpenter, An overview of heavy-atom derivatization of protein crystals, Acta Crystallogr. D Struct. Biol. 72 (Pt 3) (2016) 303–318.
[35] M. Dauter, Z. Dauter, Many ways to derivatize macromolecules and their crystals for phasing, Methods Mol. Biol. 1607 (2017) 349–356.
[36] M.A. Bukowska, M.G. Grütter, New concepts and aids to facilitate crystallization, Curr. Opin. Struct. Biol. 23 (3) (2013) 409–416.
[37] E. Sherman, J. Archer, J.D. Ye, Fab chaperone-assisted RNA crystallography (Fab CARC), Methods Mol. Biol. 1320 (2016) 77–109.
[38] N. Pujari, S.L. Saundh, F.A. Acquah, B.H.M. Mooers, A.R. Ferré-D'Amaré, A. K. Leung, Engineering crystal packing in RNA structures I: past and future strategies for engineering RNA packing in crystals, Crystals 11 (8) (2021).
[39] A.R. Ferré-D'Amaré, K. Zhou, J.A. Doudna, Crystal structure of a hepatitis delta virus ribozyme, Nature 395 (6702) (1998) 567–574.
[40] A.R. Ferré-D'Amaré, J.A. Doudna, Methods to crystallize RNA, Curr. Protocols Nucleic Acid Chem. 1 (1) (2000) 7.6.1–7.6.13.
[41] J.C. Grigg, I.R. Price, A. Ke, tRNA Fusion to Streamline RNA structure determination: case studies in probing Aminoacyl-tRNA sensing mechanisms by the T-Box Riboswitch, Cryst. 12 (5) (2022).
[42] R. Cai, I.R. Price, F. Ding, F. Wu, T. Chen, Y. Zhang, G. Liu, P.J. Jardine, C. Lu, A. Ke, ATP/ADP modulates gp16-pRNA conformational change in the Phi29 DNA packaging motor, Nucleic Acids. Res. 47 (18) (2019) 9818–9828.
[43] J. Zhang, A.R. Ferre-D'Amare, Co-crystal structure of a T-box riboswitch stem I domain in complex with its cognate tRNA, Nature 500 (7462) (2013) 363–366.
[44] L. Huang, D.M. Lilley, The molecular recognition of kink-turn structure by the L7Ae class of proteins, RNA 19 (12) (2013) 1703–1710.
[45] S. Li, Z. Su, J. Lehmann, V. Stamatopoulou, N. Giarimoglou, F.E. Henderson, L. Fan, G.D. Pintilie, K. Zhang, M. Chen, S.J. Ludtke, Y.X. Wang, C. Stathopoulos, W. Chiu, J. Zhang, Structural basis of amino acid surveillance by higher-order tRNA-mRNA interactions, Nat. Struct. Mol. Biol. 26 (12) (2019) 1094–1105.
[46] D. Dimastrogiovanni, K.S. Frohlich, K.J. Bandyra, H.A. Bruce, S. Hohensee, J. Vogel, B.F. Luisi, Recognition of the small regulatory RNA RydC by the bacterial Hfq protein, eLifeeLife 3 (2014).
[47] H. Chen, M. Egger, X. Xu, L. Flemmich, O. Krasheninina, A. Sun, R. Micura, A. Ren, Structural distinctions between NAD+ riboswitch domains 1 and 2 determine differential folding and ligand binding, Nucleic Acids. Res. 48 (21) (2020) 12394–12406.
[48] N.K. Das, N.M. Hollmann, J. Vogt, S.E. Sevdalis, H.A. Banna, M. Ojha, D. Koirala, Crystal structure of a highly conserved enteroviral 5′ cloverleaf RNA replication element, Nat. Commun. 14 (1) (2023) 1955.
[49] D. Krochmal, Y. Shao, N.S. Li, S. DasGupta, S.A. Shelke, D. Koirala, J.A. Piccirilli, Structural basis for substrate binding and catalysis by a self-alkylating ribozyme, Nat. Chem. Biol. 18 (4) (2022) 376–384.
[50] J.D. Ye, V. Tereshko, J.K. Frederiksen, A. Koide, F.A. Fellouse, S.S. Sidhu, S. Koide, A.A. Kossiakoff, J.A. Piccirilli, Synthetic antibodies for specific recognition and crystallization of structured RNA, Proc. Natl. Acad. Sci. USA 105 (1) (2008) 82–87.
[51] S.A. Shelke, Y. Shao, A. Laski, D. Koirala, B.P. Weissman, J.R. Fuller, X. Tan, T. P. Constantin, A.S. Waggoner, M.P. Bruchez, B.A. Armitage, J.A. Piccirilli, Structural basis for activation of fluorogenic dyes by an RNA aptamer lacking a G-quadruplex motif, Nat. Commun. 9 (1) (2018) 4542.
[52] H.C. Rees, W. Gogacz, N.S. Li, D. Koirala, J.A. Piccirilli, Structural basis for fluorescence activation by pepper RNA, ACS Chem. Biol. 17 (7) (2022) 1866–1875.
[53] E. Menichelli, B.J. Lam, Y. Wang, V.S. Wang, J. Shaffer, K.F. Tjhung, B. Bursulaya, T.N. Nguyen, T. Vo, P.B. Alper, C.S. McAllister, D.H. Jones, G. Spraggon, P. Y. Michellys, J. Joslin, G.F. Joyce, J. Rogers, Discovery of small molecules that target a tertiary-structured RNA, Proc. Natl. Acad. Sci. USA 119 (48) (2022), e2213117119.
[54] D.M. Shechner, R.A. Grant, S.C. Bagby, Y. Koldobskaya, J.A. Piccirilli, D.P. Bartel, Crystal structure of the catalytic core of an RNA-polymerase ribozyme, Science 326 (5957) (2009) 1271–1275.
[55] D. Koirala, S.A. Shelke, M. Dupont, S. Ruiz, S. DasGupta, L.J. Bailey, S.A. Benner, J.A. Piccirilli, Affinity maturation of a portable Fab-RNA module for chaperone-assisted RNA crystallography, Nucleic Acids. Res. 46 (5) (2018) 2624–2635.
[56] D. Koirala, Y. Shao, Y. Koldobskaya, J.R. Fuller, A.M. Watkins, S.A. Shelke, E. V. Pilipenko, R. Das, P.A. Rice, J.A. Piccirilli, A conserved RNA structural motif for organizing topology within picornaviral internal ribosome entry sites, Nat. Commun. 10 (1) (2019) 3629.
[57] H. Huang, N.B. Suslov, N.S. Li, S.A. Shelke, M.E. Evans, Y. Koldobskaya, P.A. Rice, J.A. Piccirilli, A G-quadruplex-containing RNA activates fluorescence in a GFP-like fluorophore, Nat. Chem. Biol. 10 (8) (2014) 686–691.
[58] C. Roman, A. Lewicka, D. Koirala, N.S. Li, J.A. Piccirilli, The SARS-CoV-2 programmed -1 ribosomal frameshifting element crystal structure solved to 2.09 a using chaperone-assisted RNA crystallography, ACS Chem. Biol. 16 (8) (2021) 1469–1481.
[59] D. Koirala, A. Lewicka, Y. Koldobskaya, H. Huang, J.A. Piccirilli, Synthetic antibody binding to a preorganized RNA domain of hepatitis C virus internal ribosome entry site inhibits translation, ACS Chem. Biol. 15 (1) (2020) 205–216.
[60] M. Swain, A.A. Ageeli, W.K. Kasprzak, M. Li, J.T. Miller, J. Sztuba-Solinska, J. S. Schneekloth, D. Koirala, J. Piccirili, A.J. Fraboni, R.P. Murelli, A. Wlodawer, B. A. Shapiro, N. Baird, S.F.J. Le Grice, Dynamic bulge nucleotides in the KSHV PAN ENE triple helix provide a unique binding platform for small molecule ligands, Nucleic Acids. Res. 49 (22) (2021) 13179–13193.
[61] G.J. Kapral, S. Jain, J. Noeske, J.A. Doudna, D.C. Richardson, J.S. Richardson, New tools provide a second look at HDV ribozyme structure, dynamics and cleavage, Nucleic Acids. Res. 42 (20) (2014) 12833–12846.
[62] I.A. Belashov, D.W. Crawford, C.E. Cavender, P. Dai, P.C. Beardslee, D. H. Mathews, B.L. Pentelute, B.R. McNaughton, J.E. Wedekind, Structure of HIV TAR in complex with a Lab-Evolved RRM provides insight into duplex RNA recognition and synthesis of a constrained peptide that impairs transcription, Nucleic Acids. Res. 46 (13) (2018) 6401–6415.
[63] A. Ren, Y. Xue, A. Peselis, A. Serganov, H.M. Al-Hashimi, D.J. Patel, Structural and dynamic basis for low-affinity, high-selectivity binding of L-glutamine by the glutamine riboswitch, Cell Rep. 13 (9) (2015) 1800–1813.
[64] C.P. Jones, A.R. Ferre-D'Amare, Crystal structure of a c-di-AMP riboswitch reveals an internally pseudo-dimeric RNA, EMBO J. 33 (22) (2014) 2692–2703.
[65] A. Ren, X.C. Wang, C.A. Kellenberger, K.R. Rajashankar, R.A. Jones, M. C. Hammond, D.J. Patel, Structural basis for molecular discrimination by a 3′,3′-cGAMP sensing riboswitch, Cell Rep. 11 (1) (2015) 1–12.
[66] L. Huang, J. Wang, D.M. Lilley, A critical base pair in k-turns determines the conformational class adopted, and correlates with biological function, Nucleic Acids. Res. 44 (11) (2016) 5390–5398.
[67] Y. Kondo, C. Oubridge, A.M. van Roon, K. Nagai, Crystal structure of human U1 snRNP, a small nuclear ribonucleoprotein particle, reveals the mechanism of 5′ splice site recognition, eLife 4 (2015).
[68] T. Moore, Y. Zhang, M.O. Fenley, H. Li, Molecular basis of box C/D RNA-protein interactions; cocrystal structure of archaeal L7Ae and a box C/D RNA, Structure 12 (5) (2004) 807–818.
[69] S. Hofler, P. Lukat, W. Blankenfeldt, T. Carlomagno, Eukaryotic Box C/D methylation machinery has two non-symmetric protein assembly sites, Sci. Rep. 11 (1) (2021) 17561.
[70] L. Huang, D.M. Lilley, Structure of a rare non-standard sequence k-turn bound by L7Ae protein, Nucleic Acids. Res. 42 (7) (2014) 4734–4740.
[71] L. Huang, D.M. Lilley, A quasi-cyclic RNA nano-scale molecular object constructed using kink turns, Nanoscale 8 (33) (2016) 15189–15195.
[72] K. Oshima, Y. Kakiuchi, Y. Tanaka, T. Ueda, T. Nakashima, M. Kimura, M. Yao, Structural basis for recognition of a kink-turn motif by an archaeal homologue of human RNase P protein Rpp38, Biochem. Biophys. Res. Commun. 474 (3) (2016) 541–546.
[73] T. Hamma, A.R. Ferre-D'Amare, Structure of protein L7Ae bound to a K-turn derived from an archaeal box H/ACA sRNA at 1.8 A resolution, Structure 12 (5) (2004) 893–903.
[74] S. Ashraf, L. Huang, D.M.J. Lilley, Effect of methylation of adenine N(6) on kink turn structure depends on location, RNA Biol. 16 (10) (2019) 1377–1385.
[75] J. Lin, S. Lai, R. Jia, A. Xu, L. Zhang, J. Lu, K. Ye, Structural basis for site-specific ribose methylation by box C/D RNA protein complexes, Nature 469 (7331) (2011) 559–563.
[76] J. Duan, L. Li, J. Lu, W. Wang, K. Ye, Structural mechanism of substrate RNA recruitment in H/ACA RNA-guided pseudouridine synthase, Mol. Cell 34 (4) (2009) 427–439.
[77] M.A. Schumacher, R.F. Pearson, T. Møller, P. Valentin-Hansen, R.G. Brennan, Structures of the pleiotropic translational regulator Hfq and an Hfq–RNA complex: a bacterial Sm-like protein, EMBO J. 21 (13) (2002) 3546–3556.
[78] T.M. Link, P. Valentin-Hansen, R.G. Brennan, Structure of Escherichia coli Hfq bound to polyriboadenylate RNA, Proc. Natl. Acad. Sci. 106 (46) (2009) 19292–19297.
[79] T. Someya, S. Baba, M. Fujimoto, G. Kawai, T. Kumasaka, K. Nakamura, Crystal structure of Hfq from *Bacillus subtilis* in complex with SELEX-derived RNA aptamer: insight into RNA-binding properties of bacterial Hfq, Nucleic Acids. Res. 40 (4) (2012) 1856–1867.
[80] N. Horstmann, J. Orans, P. Valentin-Hansen, S.A. Shelburne 3rd, R.G. Brennan, Structural mechanism of *Staphylococcus aureus* Hfq binding to an RNA A-tract, Nucleic Acids. Res. 40 (21) (2012) 11023–11035.
[81] W. Wang, L. Wang, Y. Zou, J. Zhang, Q. Gong, J. Wu, Y. Shi, Cooperation of *Escherichia coli* Hfq hexamers in DsrA binding, Genes Dev. 25 (19) (2011) 2106–2117.
[82] A.R. Kovach, K.E. Hoff, J.T. Canty, J. Orans, R.G. Brennan, Recognition of U-rich RNA by Hfq from the Gram-positive pathogen *Listeria monocytogenes*, RNA 20 (10) (2014) 1548–1559.
[83] L. Wang, W. Wang, F. Li, J. Zhang, J. Wu, Q. Gong, Y. Shi, Structural insights into the recognition of the internal A-rich linker from OxyS sRNA by *Escherichia coli* Hfq, Nucleic Acids. Res. 43 (4) (2015) 2400–2411.
[84] E.C. Schulz, M. Seiler, C. Zuliani, F. Voigt, V. Rybin, V. Pogenberg, N. Mucke, M. Wilmanns, T.J. Gibson, O. Barabas, Intermolecular base stacking mediates RNA-RNA interaction in a crystal structure of the RNA chaperone Hfq, Sci. Rep. 7 (1) (2017) 9903.

[85] K.A. Stanek, J. Patterson-West, P.S. Randolph, C. Mura, Crystal structure and RNA-binding properties of an Hfq homolog from the deep-branching Aquificae: conservation of the lateral RNA-binding mode, Acta Crystallogr. D Struct. Biol. 73 (Pt 4) (2017) 294–315.
[86] J. Zhang, A.R. Ferre-D'Amare, Dramatic improvement of crystals of large RNAs by cation replacement and dehydration, Structure 22 (9) (2014) 1363–1371.
[87] J.C. Grigg, A. Ke, Structural determinants for geometry and information decoding of tRNA by T box leader RNA, Structure 21 (11) (2013) 2025–2032.
[88] R.A. Battaglia, J.C. Grigg, A. Ke, Structural basis for tRNA decoding and aminoacylation sensing by T-box riboregulators, Nat. Struct. Mol. Biol. 26 (12) (2019) 1106–1113.
[89] K.C. Suddala, J. Zhang, High-affinity recognition of specific tRNAs by an mRNA anticodon-binding groove, Nat. Struct. Mol. Biol. 26 (12) (2019) 1114–1122.
[90] C. Oubridge, N. Ito, P.R. Evans, C.H. Teo, K. Nagai, Crystal structure at 1.92 Å resolution of the RNA-binding domain of the U1A spliceosomal protein complexed with an RNA hairpin, Nature 372 (6505) (1994) 432–438.
[91] S. Doublié, Preparation of selenomethionyl proteins for phase determination, Methods Enzymol. 276 (1997) 523–530.
[92] K.B. Hall, W.T. Stump, Interaction of N-terminal domain of U1A protein with an RNA stem/loop, Nucleic Acids. Res. 20 (16) (1992) 4283–4290.
[93] C.W. van Gelder, S.I. Gunderson, E.J. Jansen, W.C. Boelens, M. Polycarpou-Schwarz, I.W. Mattaj, W.J. van Venrooij, A complex secondary structure in U1A pre-mRNA that binds two molecules of U1A protein is required for regulation of polyadenylation, EMBO J. 12 (13) (1993) 5191–5200.
[94] J.C. Cochrane, S.V. Lipchock, S.A. Strobel, Structural investigation of the GlmS ribozyme bound to Its catalytic cofactor, Chem. Biol. 14 (1) (2007) 97–105.
[95] N. Kulshina, T.E. Edwards, A.R. Ferré-D'Amaré, Thermodynamic analysis of ligand binding and ligand binding-induced tertiary structure formation by the thiamine pyrophosphate riboswitch, RNA 16 (1) (2010) 186–196.
[96] B. Turner, D.M. Lilley, The importance of G.A hydrogen bonding in the metal ion- and protein-induced folding of a kink turn RNA, J. Mol. Biol. 381 (2) (2008) 431–442.
[97] D.J. Klein, T.M. Schmeing, P.B. Moore, T.A. Steitz, The kink-turn: a new RNA secondary structure motif, EMBO J. 20 (15) (2001) 4214–4221.
[98] M.T. Franze de Fernandez, W.S. Hayward, J.T. August, Bacterial proteins required for replication of phage Q ribonucleic acid. pruification and properties of host factor I, a ribonucleic acid-binding protein, J. Biol. Chem. 247 (3) (1972) 824–831.
[99] P.J. Mikulecky, M.K. Kaw, C.C. Brescia, J.C. Takach, D.D. Sledjeski, A.L. Feig, Escherichia coli Hfq has distinct interaction surfaces for DsrA, rpoS and poly(A) RNAs, Nat. Struct. Mol. Biol. 11 (12) (2004) 1206–1214.
[100] H. Makyio, J. Shimabukuro, T. Suzuki, A. Imamura, H. Ishida, M. Kiso, H. Ando, R. Kato, Six independent fucose-binding sites in the crystal structure of Aspergillus oryzae lectin, Biochem. Biophys. Res. Commun. 477 (3) (2016) 477–482.
[101] H. Huang, N.B. Suslov, N.S. Li, S.A. Shelke, M.E. Evans, Y. Koldobskaya, P.A. Rice, J.A. Piccirilli, A G-quadruplex–containing RNA activates fluorescence in a GFP-like fluorophore, Nat. Chem. Biol. 10 (8) (2014) 686–691.
[102] E. Menichelli, B.J. Lam, Y. Wang, V.S. Wang, J. Shaffer, K.F. Tjhung, B. Bursulaya, T.N. Nguyen, T. Vo, P.B. Alper, C.S. McAllister, D.H. Jones, G. Spraggon, P. Y. Michellys, J. Joslin, G.F. Joyce, J. Rogers, Discovery of small molecules that target a tertiary-structured RNA, Proc. Natl Acad. Sci. 119 (48) (2022), e2213117119.
[103] Y. Koldobskaya, E.M. Duguid, D.M. Shechner, N.B. Suslov, J. Ye, S.S. Sidhu, D. P. Bartel, S. Koide, A.A. Kossiakoff, J.A. Piccirilli, A portable RNA sequence whose recognition by a synthetic antibody facilitates structural determination, Nat. Struct. Mol. Biol. 18 (1) (2011) 100–106.
[104] M. Zuker, Mfold web server for nucleic acid folding and hybridization prediction, Nucleic Acids. Res. 31 (13) (2003) 3406–3415.
[105] J.F. Milligan, D.R. Groebe, G.W. Witherell, O.C. Uhlenbeck, Oligoribonucleotide synthesis using T7 RNA polymerase and synthetic DNA templates, Nucleic Acids. Res. 15 (21) (1987) 8783–8798.
[106] C. Kao, S. Rüdisser, M. Zheng, A simple and efficient method to transcribe RNAs with reduced 3′ heterogeneity, Methods 23 (3) (2001) 201–205.
[107] S.R. Price, N. Ito, C. Oubridge, J.M. Avis, K. Nagai, Crystallization of RNA-protein complexes. I. Methods for the large-scale preparation of RNA suitable for crystallographic studies, J. Mol. Biol. 249 (2) (1995) 398–408.
[108] A.R. Ferré-D'Amaré, J.A. Doudna, Use of cis- and trans-ribozymes to remove 5′ and 3′ heterogeneities from milligrams of *in vitro* transcribed RNA, Nucleic Acids. Res. 24 (5) (1996) 977–978.
[109] J.D. Pata, B.R. King, T.A. Steitz, Assembly, purification and crystallization of an active HIV-1 reverse transcriptase initiation complex, Nucleic Acids. Res. 30 (22) (2002) 4855–4863.
[110] K.A. Wilkinson, E.J. Merino, K.M. Weeks, Selective 2′-hydroxyl acylation analyzed by primer extension (SHAPE): quantitative RNA structure analysis at single nucleotide resolution, Nat. Protoc. 1 (3) (2006) 1610–1616.
[111] M. Till, A. Robson, M.J. Byrne, A.V. Nair, S.A. Kolek, P.D. Shaw Stewart, P. R. Race, Improving the success rate of protein crystallization by random microseed matrix screening, J. Vis. Exp. (78) (2013).
[112] M.D. Winn, C.C. Ballard, K.D. Cowtan, E.J. Dodson, P. Emsley, P.R. Evans, R. M. Keegan, E.B. Krissinel, A.G. Leslie, A. McCoy, S.J. McNicholas, G. N. Murshudov, N.S. Pannu, E.A. Potterton, H.R. Powell, R.J. Read, A. Vagin, K. S. Wilson, Overview of the CCP4 suite and current developments, Acta. Crystallogr. D Biol. Crystallogr. 67 (Pt 4) (2011) 235–242.
[113] P.D. Adams, P.V. Afonine, G. Bunkoczi, V.B. Chen, I.W. Davis, N. Echols, J. J. Headd, L.W. Hung, G.J. Kapral, R.W. Grosse-Kunstleve, A.J. McCoy, N. W. Moriarty, R. Oeffner, R.J. Read, D.C. Richardson, J.S. Richardson, T. C. Terwilliger, P.H. Zwart, PHENIX: a comprehensive Python-based system for macromolecular structure solution, Acta. Crystallogr. D Biol. Crystallogr. 66 (Pt 2) (2010) 213–221.
[114] P. Emsley, B. Lohkamp, W.G. Scott, K. Cowtan, Features and development of coot, Acta. Crystallogr. D Biol. Crystallogr. 66 (Pt 4) (2010) 486–501.